Original Article

Revealing the correlations between brain cortical characteristics and susceptibility genes for Alzheimer disease: a cross-sectional study

Liting Han[1,2#], Hanni Jiang[1,3#], Xufeng Yao[1,2], Zhe Ren[1,2], Zhongsen Qu[4], Tonggang Yu[5], Shichang Luo[1,2], Tao Wu[1]

[1]College of Medical Imaging, Jiading District Central Hospital Affiliated Shanghai University of Medicine and Health Sciences, Shanghai, China; [2]College of Health Science and Engineering, University of Shanghai for Science and Technology, Shanghai, China; [3]College of Sports and Health, Shanghai University of Sport, Shanghai, China; [4]Shanghai Sixth People's Hospital, Shanghai Jiao Tong University, Shanghai, China; [5]Shanghai Gamma Knife Hospital, Fudan University, Shanghai, China

Contributions: (I) Conception and design: L Han, X Yao, T Wu; (II) Administrative support: X Yao, T Wu; (III) Provision of study materials or patients: L Han; (IV) Collection and assembly of data: L Han, Z Ren; (V) Data analysis and interpretation: L Han, H Jiang; (VI) Manuscript writing: All authors; (VII) Final approval of manuscript: All authors.

[#]These authors contributed equally to this work.

Correspondence to: Prof. Xufeng Yao. College of Medical Imaging, Shanghai University of Medicine and Health Sciences, 279th Zhouzhu Road, Shanghai 201318, China. Email: yao6636329@hotmail.com.

Background: Alzheimer disease (AD) is a progressive neurodegenerative disease closely related to genes and characterized by the atrophy of the cerebral cortex. Correlations between imaging phenotypes and the susceptibility genes for AD, as demonstrated in the findings of genome-wide association studies (GWASs), still need to be addressed due to the complicated structure of the human cortex.

Methods: In our study, an improved GWAS method, whole cortex characteristics GWAS (WCC-GWAS), was proposed. The WCC-GWAS uses multiple cortex characteristics of gray-matter volume (GMV), cortical thickness (CT), cortical surface area (CSA), and local gyrification index (LGI). A cohort of 496 participants was enrolled and divided into 4 groups: normal control (NC; n=122), early mild cognitive impairment (EMCI; n=196), late mild cognitive impairment (LMCI; n=62), and AD (n=116). Based on the Desikan-Killiany atlas, the brain was parcellated into 68 brain regions, and the WCC of each brain region was individually calculated. Four cortex characteristics of GMV, CT, CSA, and LGI across the 4 groups optimized with multiple comparisons and the ReliefF algorithm were taken as magnetic resonance imaging (MRI) brain phenotypes. Under the model of multiple linear additive genetic regression, the correlations between the MRI brain phenotypes and single-nucleotide polymorphisms (SNPs) were deduced.

Results: The findings identified 2 prominent correlations. First, rs7309929 of neuron navigator 3 (*NAV3*) located on chromosome 12 correlated with the decreased GMV for the left middle temporal gyrus (P=0.0074). Second, rs11250992 of long intergenic non-protein-coding RNA 700 (*LINC00700*) located on chromosome 10 correlated with the decreased CT for the left supramarginal gyrus (P=0.0019).

Conclusions: The findings suggested that the correlations between phenotypes and genotypes could be effectively evaluated. The strategy of extracting MRI phenotypes as endophenotypes provided valuable indications in AD GWAS.

Keywords: Alzheimer disease (AD); cortex characteristics; susceptibility genes; genome-wide association study (GWAS); phenotypes

Submitted Jun 14, 2022. Accepted for publication Feb 20, 2023. Published online Mar 22, 2023.
doi: 10.21037/qims-22-602
View this article at: https://dx.doi.org/10.21037/qims-22-602

Introduction

Alzheimer disease (AD) is an age-related neurodegenerative disorder mostly accompanied by progressive memory loss, impaired executive function, and other related clinical symptoms (1). The incidence of AD increases with age, and the total number of affected people worldwide will exceed 100 million by 2030 (2). AD seriously affects the quality of life of patients and leverages a heavy burden on society and families. The occurrence of AD is closely related to genetic factors and is characterized by atrophy of the brain cortex (3). The imaging genomics of AD has recently become a research hotspot.

Imaging genomics is a promising research field that could not only help to discover the biomarkers of AD but also investigate the impact of human genetic variation on the structure, chemistry, and function of neural systems at the genome-wide level. Imaging genomics can even reveal the complex interaction between genetic variants and phenotypic imaging features. Thus, imaging genomics has aroused the interest of many researchers. Unlike the two other approaches of imaging genomics, hybrid algorithms have a greater capacity to exploit the statistical power and biological interpretation in formulating a decisive diagnosis and prognosis for AD (4,5).

As AD progresses, the topological changes in brain structure can be detected using a variety of imaging techniques. Since structural magnetic resonance imaging (sMRI) possesses the preponderant capability of accurately reflecting the morphological changes of the cortex, whole cortex characteristics (WCC) is regarded as a critical phenotype in imaging genomics (6-8). Notably, the WCC of gray-matter volume (GMV), cortical thickness (CT), cortical surface area (CSA), and local gyrification index (LGI) has been measured to investigate the brain cortical changes of AD (9-11). It was reported that the changes in CT and CSA in the bilateral hemispheres demonstrated a significant decrease in the AD group compared with those in the mild cognitive impairment (MCI) and normal control (NC) groups (12). Moreover, the cortex characteristics of CT and CSA at the frontal, temporal, and occipital lobes show significant reduction starting at the temporal lobe and gradually expanding to the whole brain as AD progresses. Another study, reported there to be an obvious decrease in the global GMV in an AD group compared with an MCI group (13). In general, the WCC can demonstrate specific indications of cortical changes, and those characteristics could be used as potential imaging markers or phenotypes to predict AD (14).

In order to search for causative genes or genotypes, the genomic approaches proceed through stages of candidate gene-based association studies, genome-wide association studies (GWASs), and next-generation sequencing. Unlike the limited effect sizes of single quantitative trait associations, the GWAS possesses the ability to simultaneously identify genetic variant polymorphisms across the genome at the population level of AD (15,16). Earlier studies found that the single-nucleotide polymorphism (SNP) rs4420638 on chromosome 19, located 14 kilobase pairs distal to apolipoprotein E (*APOE*) ε4, could significantly differentiate AD cases from controls and was more strongly associated with the risk of AD than any other SNPs of those tested (17). A large 2-stage meta-analysis of GWAS revealed that the gene *ZCWPW1* had the strongest association with the 11 new AD-related susceptibility loci as the corresponding proteins of the introns modulated epigenetic regulation (18). Further studies discovered 29 more susceptibility genes in data sets with large samples (19,20). Among them, the most prominent genes, *ADAM10*, *BCKDK/KAT8*, and *ACE*, were connected with the deposition of amyloid beta, the increased risk of AD, and the atrophy of the hippocampus and amygdala, respectively. Although GWAS has been used to identify many risk genes, the biological mechanisms and function of genetic variants remain to be elucidated (21,22).

A variety of GWAS strategies have been proposed to reveal the correlations between imaging phenotypes and genotypes for AD (23,24). CT, one of the most sensitive imaging biomarkers of structural brain atrophy in AD, was selected as an endophenotype and was found to be strongly correlated with 4 genes (*B4GALNT1*, *RAB44*, *LOC101927583*, and *SLC26A10*) related to protein degradation, neuronal deletion, and apoptosis (25,26). Another GWAS study showed that the medial temporal circuit (MTC) could be used as another imaging phenotype and that the SNP rs34173062 in the *SHARPIN* gene had a

genetic modifying effect on MTC atrophy (27). Recently, it was demonstrated that the SNP rs661526 modulated the expression of *NFIA* in the substantia nigra and the frontal cortex (FCTX), and the SNP rs10109716 modulated the expression of *ST18* in the thalamus, which were significantly associated with increased CT in the left parahippocampal gyrus and left inferior frontal gyrus, respectively (28). Moreover, multiple imaging phenotypes acquired by MRI and positron emission tomography (PET), including increased cortical amyloid burden and bilateral hippocampal volume atrophy, were determined to be associated with the rs6850306 in AD and other neurodegenerative diseases (29).

However, the existing studies did not fully consider the WCC as imaging phenotypes in the GWAS studies. Failing to do so neglects some of the potential phenotypes which could reflect the complicated cortical changes in the human brain (30). Therefore, correlations between WCC and susceptibility genes should be investigated to deepen the understanding of the pathogenesis and heritability of AD.

In our study, we proposed an imaging genomics approach, WCC-GWAS, to reveal the relationships between imaging phenotypes and SNP genotypes for the detection of biological markers in AD. In our method, the WCC of GMV, CT, CSA, and LGI were implemented to investigate the effect of the susceptibility genes on cortical changes. The novelty of our study is as follows: (I) we are the first to use the WCC of GMV, CT, CSA, and LGI for the selection of imaging phenotypes via the hybrid algorithms of 1-way analysis of variance (ANOVA) and ReliefF; and (II) the correlations of imaging genomics were verified using the evaluation of expression quantitative trait loci (eQTL), and the functional effect of genetic variants on the gene expression were identified for the public gene database. We present the following article in accordance with the STREGA reporting checklist (available at https://qims.amegroups.com/article/view/10.21037/qims-22-602/rc).

Methods

Study design

In our experimental setup, 4 experiments were conducted to validate the robustness of WCC-GWAS. First, the WCC of 4 groups was chosen as the MRI phenotype across the 4 groups. Second, Pearson correlation analyses were used to evaluate the relationships between MRI cortex phenotypes and cognitive scales of mini-mental state examination (MMSE), clinical dementia rating sum of boxes (CDR-SB), and functional activities questionnaire (FAQ) scores, respectively. Third, the correlation analyses of GWAS were conducted to reveal the relationships of imaging genomics. Finally, eQTL analysis was used to verify the expected results for the GWAS correlations.

Participants

Data used in this article were obtained from the database of the Alzheimer's Disease Neuroimaging Initiative (ADNI) (http://adni.loni.usc.edu) (31). Specifically, information including age, sex, years of education, the number of *APOE* ε4 carriers (2 or 1 or no copies of allele 4), SNP genotype data, sMRI, cognitive scores of the MMSE), CDR-SB, and FAQ were measured at the baseline. In this study, a cohort of 526 participants was recruited from the 2016 ADNI GO/2 for retrospective analysis. The enrollment criteria for participants were as follows: age range, 55–90 years old; visual and auditory capabilities with adequate acuity for neuropsychological testing; no severe medical, neurological, or psychiatric disease; no history of significant head trauma; no non-AD-related pharmaceuticals known to affect brain function, and alcohol or drug addiction; not pregnant, lactating, or with the potential for childbearing; completed 6 grades of education or had a good work history; spoke English or Spanish fluently; agreed to have blood samples collected for GWAS, APOE testing, and DNA and RNA banking; and agreed to have blood samples collected for biomarker testing and at least 1 lumbar puncture for cerebrospinal fluid. This retrospective study was conducted in accordance with the Declaration of Helsinki (as revised in 2013) and was approved by the ethics committee of Shanghai University of Medicine and Health Sciences. Individual consent for this retrospective analysis was waived.

Gene sequencing and image acquisition

The image and gene data were acquired with MRI scanning and gene sequencing. The genotyping was performed using the Illumina HumanOmniExpress BeadChip in ADNI GO/2, and intensity data were processed with GenomeStudio v. 2009.1. This approach enabled versatile custom genotyping, flexible content design, and high throughput capabilities with high data quality. There were 709,358 SNPs left for the 526 cases after gene testing. All MRI examinations were conducted using 3-Tesla (3T) MRI scanners. The standard sequence of 3-dimensional high-resolution T1-weighted imaging (T1WI) protocols were

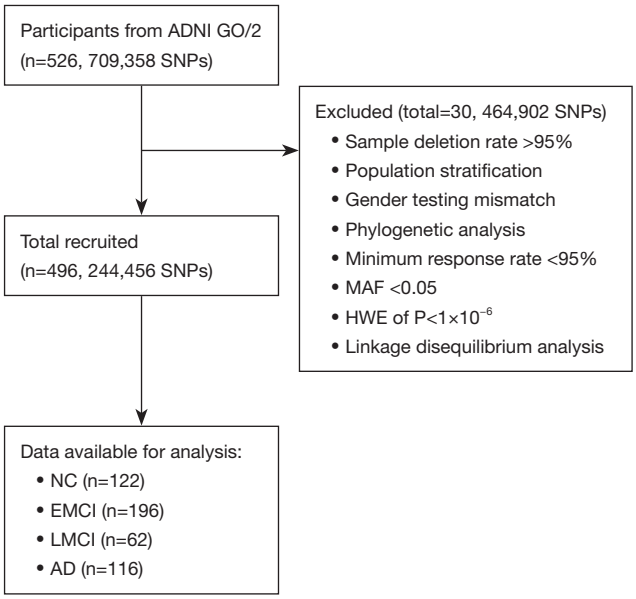

Figure 1 Participant recruitment flow diagram. ADNI, Alzheimer's Disease Neuroimaging Initiative; SNP, single-nucleotide polymorphism; MAF, minor allele frequency; HWE, Hardy-Weinberg equilibrium; NC, normal control; EMCI, early mild cognitive impairment; LMCI, late mild cognitive impairment; AD, Alzheimer disease.

acquired using the standard head phased-array coils with at least 16 channels. The scanning parameters were as follows: time of repetition (TR), 2,300 ms; time of echo (TE), 2.98 ms; field of view (FOV), 240×240 mm^2; slice thickness, 1.2 mm; and acquisition matrix, 256×256.

WCC-GWAS approach

In our study, an imaging genomics approach, WCC-GWAS, was proposed for correlation analyses between imaging phenotypes and genotypes. This approach consisted of 5 steps: quality control of genetic and MRI data, grouping description, phenotypic computation, correlations of phenotypes and genotypes, and eQTL analysis.

Quality control of genetic and MRI data

The standard quality control of genotype data included the following: sample deletion rate <95%, minimum response rate >95%, Hardy-Weinberg equilibrium (HWE) of $P>1\times10^{-6}$, minor allele frequency (MAF) >0.05, gender testing, linkage disequilibrium analysis, and population stratification with principal component analysis (PCA). Finally, the 244,456 SNPs of 496 participants were chosen as genotypic SNPs. *Figure 1* shows the screening process of participants. The quality control of genetic data was conducted with the PLINK 1.9 software (https://www.cog-genomics.org/plink/1.9) (32). Additionally, the MRI data of enrolled participants were visually inspected for the details of image quality. This process guaranteed the integrity and consistency of the genetic and MRI data for the retrospective study.

Grouping description

According to the National Institute of Neurological and Communicative Disorders and Stroke-Alzheimer's Disease and Related Disorders Association (NINCDS-ADRDA) criteria (33), the 496 participants were divided into 4 groups: NC (122 cases), early mind cognition impairment (EMCI; 196 cases), late mind cognition impairment (LMCI; 62 cases), and AD (116 cases).

Phenotypic computation

The MRI phenotypic characteristics were obtained by phenotypic computation across the 4 groups. This process mainly contained 3 steps: measurement of WCC, statistical optimization, and ReliefF sorting.

First, the measurement of WCC consisted of the following: normalization, nonuniform field correction, removal of nonbrain tissues, segmentation of GM and white matter, topological correction, surface construction, expansion filling of cerebrospinal fluid, atlas registration, and computation of WCC. According to the Desikan-Killiany atlas, the WCC of GMV, CT, CSA, and LGI were calculated for 68 brain regions. These data were processed with Freesurfer 5.1.0 software (https://surfer.nmr.mgh.harvard.edu/pub/dist/freesurfer/5.1.0) (34).

Second, statistical optimization was used to extract significant cortex characteristics from WCC. To ensure the normal distribution and homogeneity of MRI phenotypic characteristics, the Shapiro-Wilk test and histograms for the normal distribution and the variance homogeneity test for the variance homogeneity were performed, respectively. Then, the analysis of 1-way ANOVA was used to compare the GMV, CT, CSA, and LGI of 68 brain regions among all groups. A total of 125 significant cortex characteristics were chosen from the 272 cortex characteristics, as listed in Table S1 ($P<0.001$).

Table 1 Demographics and clinical scores of enrolled participants (mean ± SD)

Variables	NC (n=122)	EMCI (n=196)	LMCI (n=62)	AD (n=116)	P value
Age (years)	74.54±5.60	71.33±7.35	72.64±7.71	74.81±8.19	<0.05*
Sex (female/male)	61/61	86/110	24/38	46/70	>0.05
Education (years)	16.43±2.53	15.83±2.62	16.63±2.54	15.70±2.68	<0.05*
APOE ε4 (0/1/2)	90/28/4	117/66/13	30/25/7	39/56/21	<0.05*
CDR-SB	0.04±0.15	1.25±0.78	1.78±1.05	5.25±2.10	<0.05*
MMSE	28.98±1.29	28.32±1.54	27.65±1.95	22.19±3.26	<0.05*
FAQ	0.16±0.63	1.89±3.15	4.53±5.09	16.16±7.09	<0.05*

*, significant statistical level of P<0.05. SD, standard deviation; NC, normal control; EMCI, early mild cognitive impairment; LMCI, late mild cognitive impairment; AD, Alzheimer disease; APOE ε4, apolipoprotein E ε4; CDR-SB, clinical dementia rating sum of boxes; MMSE, mini-mental state examination; FAQ, functional activities questionnaire.

Third, the algorithm of ReliefF was applied to determine the most critical cortex characteristics from the significant cortex characteristics mentioned above (35). This process was performed because the ReliefF could detect the context information among features, and the weights of WCC were sorted according to the relevance between features and categories (36). In total, a set of 14 cortex characteristics was chosen as MRI phenotypes at the threshold of 0.015.

Correlations of phenotypes and genotypes

The correlations between the 14 MRI phenotypes and 244,456 genotypic SNPs were analyzed using additive genetic linear regression with PLINK 1.9 software. Here, the variables of age, sex, years of education, the top 10 weights of PCA, and the number of *APOE* ε4 carriers were taken as covariates. Two thresholds were chosen: $P<1\times10^{-5}$ for the suggestive association threshold and $P<5\times10^{-8}$ for the genome-wide significance. To verify the multiple hypothesis testing, the Benjamini-Hochberg (BH) procedure was used, and the false discovery rate (FDR) control was implemented using the "p.adjust()" function, a base package that comes with R 4.2 software (The R Foundation for Statistical Computing; https://www.r-project.org) to guarantee the accuracy of the results (P*<0.05) (37). The potential SNPs were required to pass the FDR control threshold (P*<0.05), while the top SNPs were required to pass the genome-wide significance threshold ($P<5\times10^{-8}$). Moreover, the significant correlations of phenotypes and genotypes were visualized with Manhattan and quantile-quantile (Q-Q) plots drawn with the "qqman" package in R 4.2 software. Accordingly, the adjacent regions and genetic information of significant SNPs were drawn with LocusZoom Python application.

eQTL analysis

In our experiment, the eQTL analysis was used to study the correlation between genetic mutation and gene expression by using gene expression as a trait. To identify the functional effect of genetic variants on the gene expression, the correlations between genotypes and gene expression in 10 brain tissues were verified on the Brain eQTL Almanac (Braineac) database (the FDR correction was performed as described in the Correlations of phenotypes and genotypes section; P<0.05) (38). The Braineac database is a public database consisting of 134 people of European descent who do not have neurodegenerative diseases. The genotypes and gene expression levels in 10 brain regions could be used to verify the SNPs in genes associated with neurological disorders.

Results

Demographic and clinical characteristics

The demographic details and clinical scores of the 4 groups are displayed in *Table 1*. The statistical analyses of 1-way ANOVA and the chi-squared test were performed to compare the demographic differences among the 4 groups (P<0.05) (39).

Results of MRI cortex phenotypes

The details of the 14 MRI phenotypes of AD are listed in *Table 2*. There were 12 MRI cortex phenotypes of CT,

Table 2 Details of the14 MRI phenotypes (mean ± SD)

Phenotypes	NC	EMCI	LMCI	AD
CT (mm)				
Left entorhinal	3.3159±0.2947	3.2374±0.4231	3.0066±0.4965	2.6428±0.4535
Right entorhinal	3.4922±0.3335	3.4044±0.5123	3.1768±0.5631	2.8315±0.5293
Left superior temporal gyrus	2.6017±0.1386	2.6066±0.1900	2.5123±0.0456	2.4081±0.1691
Right superior temporal gyrus	2.6087±0.1415	2.6149±0.1788	2.5631±0.1626	2.4582±0.1612
Left middle temporal gyrus	2.7050±0.1313	2.7036±0.1483	2.6558±0.1964	2.5343±0.1963
Right middle temporal gyrus	2.7425±0.1254	2.7246±0.1713	2.7177±0.1640	2.5737±0.1971
Left precuneus	2.2057±0.1295	2.2122±0.1445	2.1631±0.1509	2.0783±0.1587
Right precuneus	2.2407±0.1248	2.2627±0.1289	2.2083±0.1273	2.0994±0.1635
Left inferior parietal gyrus	2.2683± 0.1214	2.2786±0.1312	2.2357±0.1498	2.1332±0.1825
Right fusiform gyrus	2.6121±0.1409	2.6160±0.1651	2.5689±0.2044	2.4537±0.2015
Left supramarginal gyrus	2.3761±0.1236	2.3934±0.1334	2.3560±0.1508	2.2517±0.1584
Right isthmus of cingulate gyrus	2.2966±0.2122	2.3203±0.2076	2.2333±0.2599	2.1409±0.2136
GMV (mm^3)				
Left middle temporal gyrus	9,508.5±1,166.9	9,837.2±1,446.7	8,987.6±1,472.1	8,295.6±1,576.7
Left entorhinal	1,751.2±358.00	1,776.2±429.45	1,554.9±390.53	1,341.4±443.78

MRI, magnetic resonance imaging; SD, standard deviation; NC, normal control; EMCI, early mild cognitive impairment; LMCI, late mild cognitive impairment; AD, Alzheimer disease; CT, cortical thickness; GMV, gray-matter volume.

left entorhinal, right entorhinal, left superior temporal gyrus, right superior temporal gyrus, left middle temporal gyrus, right middle temporal gyrus, left precuneus, right precuneus, left inferior parietal gyrus, left supramarginal gyrus, right fusiform gyrus, and right isthmus of the cingulate gyrus. The CT gradually decreased from NC to AD, and there was an especially obvious decrease from LMCI to AD (P<0.001). The 2 MRI cortex phenotypes of GMV (left entorhinal and left middle temporal gyrus) first had a marginal increase from NC to EMCI and then slowly decreased from EMCI to AD (P<0.001).

Pearson correlation analyses

The results shown in *Table 3* demonstrated that the 14 MRI phenotypes were significantly correlated with the neuropsychological scale scores ($0.2 < |r| < 0.6$; P<0.001). These results suggested that these phenotypes did have strong specificity with the cognitive scales across the 4 groups.

Results of GWAS correlations

With the suggestive association threshold ($P<1\times10^{-5}$), 31 SNPs were reserved. Moreover, 2 top SNPs (rs7309929 and rs11250992) passed the genome-wide significance threshold ($P<5\times10^{-8}$). After FDR correction on the 31 SNPs, 4 SNPs passed the FDR control threshold (P*<0.05), including 2 top SNPs (rs7309929 and rs11250992) and 2 potential SNPs (rs2803433 and rs17669844), as shown in *Table 4*. The top SNP of rs7309929 was strongly associated with the reduction of GMV in the left middle temporal gyrus ($P=3.04\times10^{-8}$). The top SNP of rs11250992 was strongly associated with the reduction of CT in the left supramarginal gyrus ($P=7.90\times10^{-9}$) and weakly correlated with the reduction of CT in the left superior temporal gyrus. The 2 potential SNPs of rs2803433 and rs17669844 had weak associations with CT reduction in the left supramarginal gyrus and right isthmus of the cingulate gyrus, respectively.

Figure 2A shows that 3 SNPs (rs7579742, rs7048339, and rs7309929) passed the suggestive association threshold

Table 3 Relationships between CT of specific brain regions and the scores of the cognitive scales MMSE, CDR-SB, and FAQ

Phenotypes	MMSE		CDR-SB		FAQ	
	r	P value	r	P value	r	P value
CT						
Left entorhinal	0.481	<0.001	−0.466	<0.001	−0.500	<0.001
Right entorhinal	0.389	<0.001	−0.417	<0.001	−0.460	<0.001
Left superior temporal gyrus	0.429	<0.001	−0.369	<0.001	−0.429	<0.001
Right superior temporal gyrus	0.342	<0.001	−0.318	<0.001	−0.375	<0.001
Left middle temporal gyrus	0.366	<0.001	−0.352	<0.001	−0.417	<0.001
Right middle temporal gyrus	0.318	<0.001	−0.331	<0.001	−0.374	<0.001
Left precuneus	0.312	<0.001	−0.316	<0.001	−0.343	<0.001
Right precuneus	0.350	<0.001	−0.350	<0.001	−0.405	<0.001
Left inferior parietal gyrus	0.346	<0.001	−0.330	<0.001	−0.383	<0.001
Right fusiform gyrus	0.316	<0.001	−0.306	<0.001	−0.387	<0.001
Left supramarginal gyrus	0.331	<0.001	−0.308	<0.001	−0.364	<0.001
Right isthmus of cingulate gyrus	0.254	<0.001	−0.274	<0.001	−0.342	<0.001
GMV						
Left middle temporal gyrus	0.356	<0.001	−0.316	<0.001	−0.340	<0.001
Left entorhinal	0.376	<0.001	−0.367	<0.001	−0.375	<0.001

r, Pearson correlation coefficient. CT, cortical thickness; MMSE, mini-mental state examination; CDR-SB, clinical dementia rating sum of boxes; FAQ, functional activities questionnaire; GMV, gray-matter volume.

Table 4 Results of GWAS correlations

Significant SNPs	CHR	Gene	SNP location	MAF	P	P*	Regions-phenotypes
rs7309929	12	NAV3	Intronic variant	0.286	3.04×10^{-8}	0.0074	Left middle temporal gyrus-GMV
rs11250992	10	LINC00700	Upstream transcript variant	0.483	7.90×10^{-9}	0.0019	Left supramarginal gyrus-CT
					6.43×10^{-8}	0.0157	Left superior temporal gyrus-CT
rs2803433	9	PCSK5	Intronic variant	0.123	1.39×10^{-7}	0.0169	Left supramarginal gyrus-CT
rs17669844	7	CREB5	Intronic variant	0.289	1.79×10^{-7}	0.0438	Right isthmus of cingulate gyrus-CT

P, P value for GWAS level; P*, P value after FDR correction. GWAS, genome-wide association study; SNP, single-nucleotide polymorphism; CHR, chromosome; MAF, minor allele frequency; NAV3, neuron navigator 3; GMV, gray-matter volume; LINC00700, long intergenic non-protein-coding RNA 700; CT, cortical thickness; PCSK5, proprotein convertase subtilisin/Kexin type 5; CREB5, CAMP responsive element binding protein 5; FDR, false discovery rate.

(the blue line). Only 1 top SNP of rs7309929 located at the *NAV3* gene on chromosome 12 passed the genome-wide significance threshold (the red line), and the 2 other SNPs (rs7579742 and rs7048339) did not pass the FDR control. *Figure 2B* shows that 4 SNPs (rs2803433, rs11952661, rs503422, and rs11250992) passed the suggestive association threshold (the blue line). Furthermore, 1 top SNP (rs11250992) located at the gene *LINC00700* on chromosome 10 passed the genome-wide significance threshold (the red line), 1 potential SNP (rs2803433) passed FDR control, and 2 other SNPs (rs11952661 and rs503422) did not pass the FDR control. Here, the blue line represents

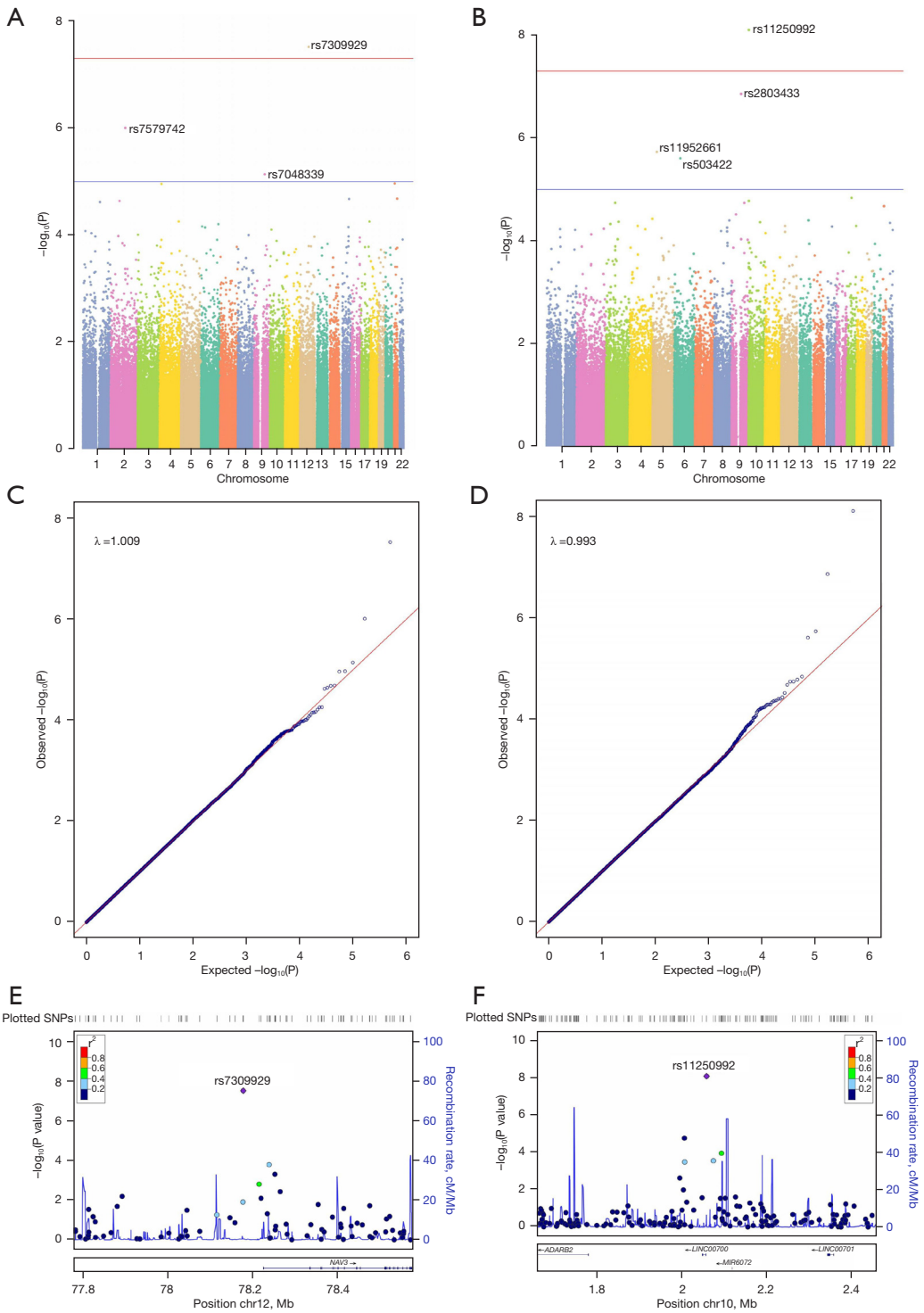

Figure 2 Interpretation of GWAS correlations. (A,B) Manhattan maps of the results of the GWAS in the GMV of the left middle temporal gyrus and the CT of the left supramarginal gyrus, respectively. (C,D) Q-Q plots of comparison of the observed and expected values of the GMV of the left middle temporal gyrus and the CT of the left supramarginal gyrus, respectively. (E,F) Regional association maps of the regional linkage imbalance for rs7309929 (±400 kB) and rs11250992 (±400 kB), respectively. SNP, single-nucleotide polymorphism; GWAS, genome-wide association study; GMV, gray-matter volume; CT, cortical thickness; Q-Q plots, quantile-quantile plots.

the suggestive association threshold (1×10^{-5}), and the red line represents the genome-wide association threshold (5×10^{-8}). The Q-Q plots of the left middle temporal gyrus and the left supramarginal gyrus were used to compare the observed and expected P values (*Figure 2C*,*2D*). The genomic inflation factor of the 2 top SNPs were 1.009 and 0.993, respectively. The results indicated there to be no remarkable inflation of the observed P value or population stratification phenomenon. Furthermore, the regional association maps showed that there was no SNP in high linkage disequilibrium between the 2 top SNPs (*Figure 2E*,*2F*).

The correlations between significant SNPs and MR brain phenotypes are shown in *Figure 3*. rs7309929 (C/T) was significantly correlated with the GMV of the left middle temporal gyrus (P=0.007), the C allele carriers of the rs7309929 demonstrated a decreased tendency of GMV (CT > TT > CC), rs11250992 (G/T) was significantly correlated with the CT of the left supramarginal gyrus (P=0.002) and left superior temporal gyrus (P=0.02), the G allele carriers of the rs11250992 (G/T) gradually decreased for CT (TT > GT > GG), rs2803433 (C/T) was significantly correlated with the CT of the left supramarginal gyrus (P=0.02), the CT became thinner in the C allele carriers (TT > CT > CC), rs17669844 (A/G) was significantly correlated with the CT of the right isthmus of the cingulate gyrus (P=0.04), and the A allele carriers of the rs17669844 had a decreased CT (GG > AG > AA).

Results of eQTL analysis

Since there were no cases of expression of the *LINC00700* gene in the Braineac database, 3 candidate loci (*NAV3*, *PCSK5*, and *CREB5*) were selected, and their corresponding SNPs (rs7309929, rs2803433, and rs17669844) were used for the eQTL analysis. It was clear that there were 4 increased expressions, including the T allele of rs7309929 for *NAV3* in the substantia nigra (SNIG; P=0.002, probe set 3423384), the A allele of rs2803433 for *PCSK5* in the cerebellar cortex (CRBL; P=0.006, probe set 3175293), the G allele for *PCSK5* in the prefrontal cortex (P=0.03, probe set 3175293), and the T allele in rs17669844 for *CREB5* in the FCTX (P=0.02, probe set 2994646), as shown in *Figure 4*.

Discussion

AD is the most common type of dementia, but the pathological mechanism remains unclear. In our study, we proposed an improved WCC-GWAS to analyze the correlations between imaging phenotypes and genotypes. This approach can deepen the understanding of the pathophysiological mechanism of AD by revealing the effect of genetic loci on cortex characteristics.

In our study, the WCC of GMV, CT, CSA, and LGI were used to accurately reflect the cortical alternations. A previous study showed that AD classification via multiparameter combination (i.e., GMV, CT, and CSA) obtained the optimal accuracy of 90.76% for the support vector machine classifier (40). Pronounced brain regions for CT decline were located in the temporal and limbic lobes, whereas those for GMV and CSA were distributed in more diffuse regions of the brain (11). Except for the GMV, CT, and CSA, the LGI also demonstrated obvious changes in the measurement of the brain cortex for AD progression. Furthermore, in subjective cognitive impairment, the left lingual gyrus showed a significant reduction of LGI (41). The multiple phenotypes could provide detailed information about complex morphological changes in cortical structures.

Our experiments pointed to 4 loci, rs7309929, rs11250992, rs2803433, and rs17669844, as potential genetic risk loci for AD. The rs11250992 in *LINC00700* influenced not only the CT of the left supramarginal gyrus but also the CT of the left superior temporal gyrus. This finding suggests that the single locus produces complicated effects on multiple imaging phenotypes. However, the possible role of this gene has not been reported in GWAS studies. These findings show that the vital role of SNPs can be explained by regional specificity and are not limited to an individual region in relation to AD pathogenesis (42).

Another locus, rs7309929, was labeled as one of the hotspot SNPs. It was located on chromosome 12 and belonged to the intronic variant region of the *NAV3* gene. Similar to how *UNC-53* regulates T-cell production of interleukin-2 (IL2), *NAV3* is a protein-coding gene that is mainly expressed in the nervous system and involved in neuronal regeneration (43). Other studies have found that, during the neurodegenerative process of AD, the expression of *NAV3* was predominantly enhanced in the degenerated pyramidal neurons of the cerebral cortex (44). This is consistent with our findings, which showed that the rs7309929 of *NAV3* was correlated with the GMV for the left middle temporal gyrus. The collateral homolog of *NAV3*, *NAV2*, was identified as a new risk gene and correlated with the episodical memory rating scale for

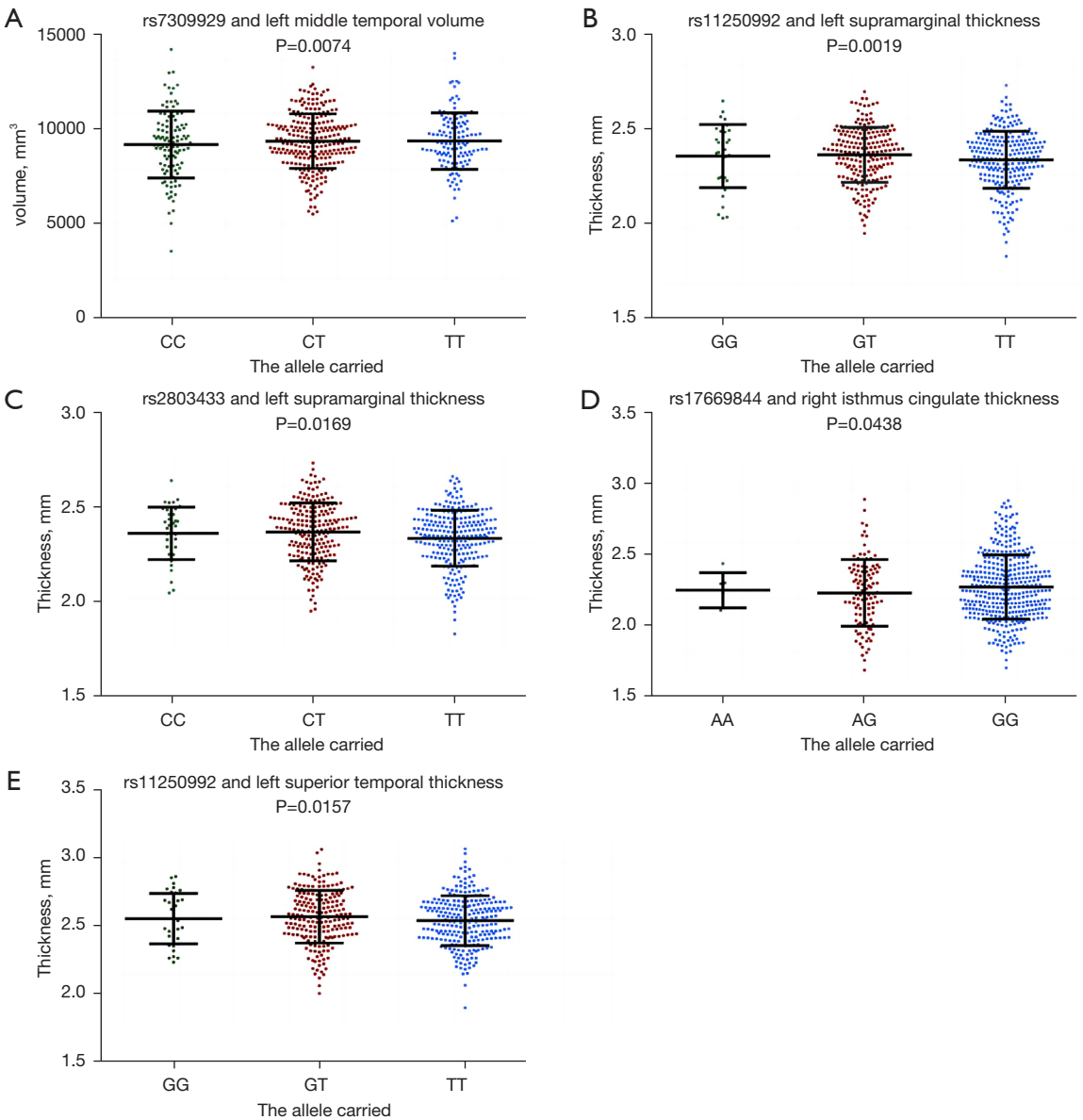

Figure 3 Correlations between significant SNPs and MRI brain phenotypes. (A) Correlation between GMV of the left middle temporal gyrus and rs7309929. (B) Correlation between CT of the left supramarginal gyrus and rs11250992. (C) Correlation between CT of the left supramarginal gyrus and rs2803433. (D) Correlation between CT of the right isthmus of cingulate gyrus and rs17669844. (E) Correlation between CT of the left superior temporal gyrus and rs11250992. SNP, single-nucleotide polymorphism; MRI, magnetic resonance imaging; GMV, gray-matter volume; CT, cortical thickness.

AD (45,46). Overall, these results point to *NAV3* as likely having a specific role in neurite growth and cell migration, which should be investigated further in studies of AD.

One of the hotspot SNPs was rs2803433, located in the proprotein convertase subtilisin/Kexin type 5 (*PCSK5*) gene on chromosome 9. It is well-known that the *PSCK* family plays a major physiological role during development and adulthood. The *PCSK5* gene regulates the levels of endothelial lipases, lipoprotein lipases, and low-density lipoprotein receptors by regulating the breakdown of *PCSK9*, thereby affecting lipoprotein metabolism (47). The polymorphisms of the *PCSK5* gene have been associated

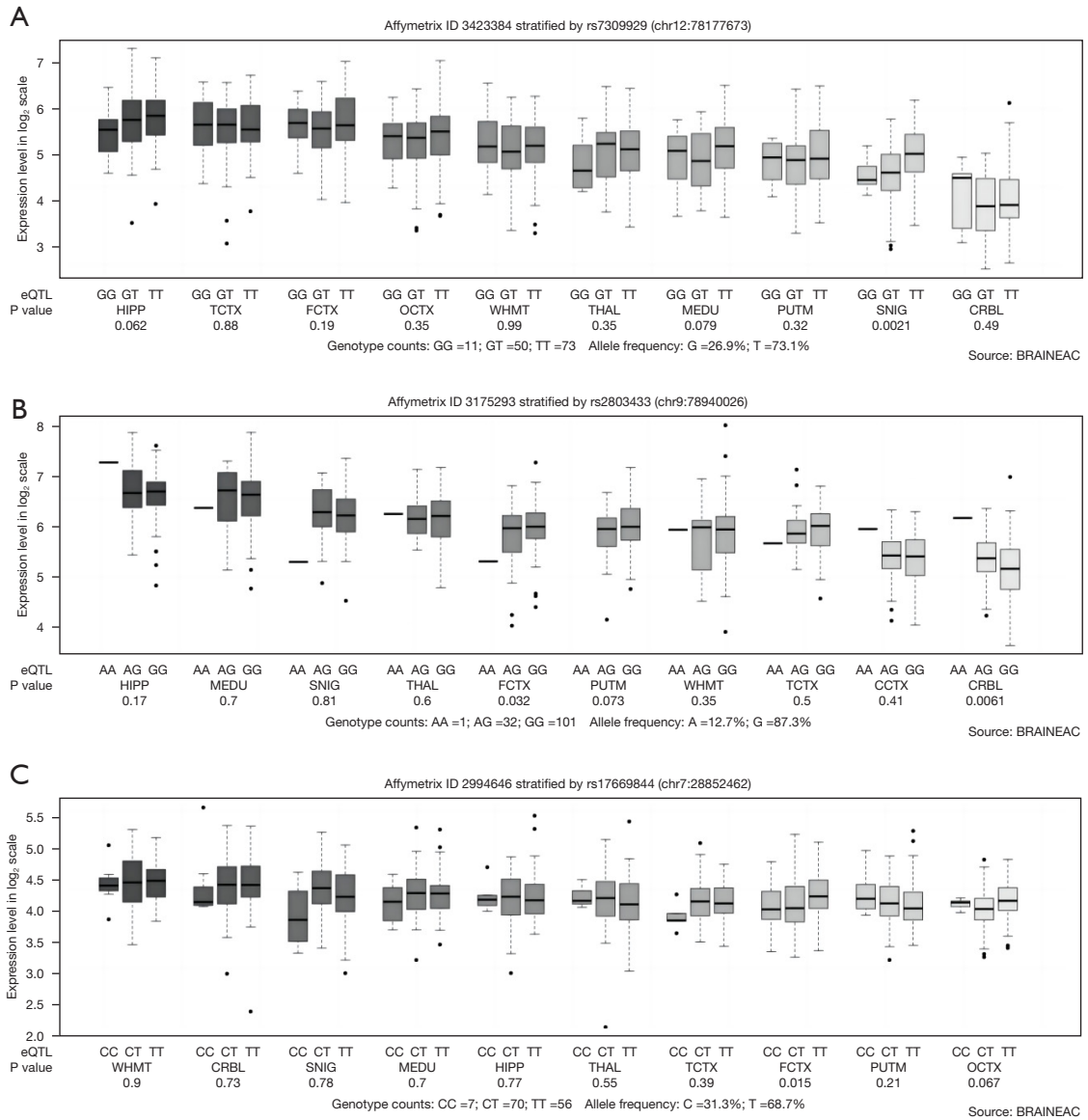

Figure 4 The effect of the top SNPs on genetic expression. (A) The T allele of rs7309929. (B) The A allele of rs2803433. (C) The T allele in rs17669844. ID, identity document; chr, chromosome; eQTL, expression quantitative trait loci; HIPP, hippocampus; TCTX, temporal cortex; FCTX, frontal cortex; OCTX, occipital cortex; WHMT, white matter; THAL, thalamus; MEDU, medulla; PUTM, putamen; SNIG, substantia nigra, CRBL, cerebellum; BRAINEAC, Brain eQTL Almanac; SNP, single-nucleotide polymorphism.

with phenotypes for humans and mutations in a variety of diseases, such as hypercholesterolemia and hypotension (48,49). Other research reported that the expression of the *PCSK* enzyme was regulated by genetic factors and could be used as a potential genetic risk locus of AD (42).

In addition, rs17669844 located on chromosome 7 belonged to the intronic region of the CAMP responsive element binding protein 5 (*CREB5*) and impaired the signaling routes in diseases, such as cognitive deficits of Parkinson disease and AD. For DNA methylation, *CREB5*-hypomethylated changes may accelerate neuronal death and are closely related to AD (50,51).

The eQTL analysis could identify the loci that expressed quantitative traits. In the Braineac database, the loci

rs7309929, rs2803433, and rs17669844 were found to affect the gene expressions of *NAV3*, *PCSK5*, and *CREB5*, respectively. These results indicate that the polymorphism of susceptibility genes might influence gene expression and accelerate the occurrence of AD. To date, traditional machine learning approaches, including deep learning, have been used to distinguish AD in gene expression data (52,53). The findings demonstrated the potential of susceptibility genes being used as biomarkers for predicting AD progression. The use of eQTL database allowed us to better understand the relationship between human gene expression and genetic variation. In doing so, this study provides an opportunity to explain the candidate genes for AD.

This study had several limitations. First, the results were obtained from a variety of MRI scanner types across multiple centers. The sMRI cortical measurements can be easily affected by minor differences in MRI hardware, scanning sequences, and processing details. The consistency of sMRI sequences of MRI vendors is difficult to evaluate due to a lack of a gold standard. More exhaustive studies on different MRI scanners may be needed to form more convincing conclusions. Second, we restricted the analysis to participants who were only of European ancestry. The composition of our samples makes it difficult to generalize our findings to other populations. However, to the best of our knowledge, there are no other public AD databases comprising adequate and comprehensive image and gene data, and a systematic study on this issue is not currently feasible.

Conclusions

The proposed WCC-GWAS could be used effectively to investigate the correlations of imaging genomics. The genes identified in this study play a critical role in sMRI-based alteration in WCC, and studying them will provide further insights into the genetic mechanism of AD.

Acknowledgments

Funding: This project was funded by the National Natural Science Foundation of China (Nos. 61971275 and 81830052), the National Key Research and Development Program of China (No. 2020YFC2008700), and the Shanghai Municipal Commission of Science and Technology for Capacity Building for Local Universities (No. 23010502700). Data collection and sharing for this project were funded by the Alzheimer's Disease Neuroimaging Initiative (ADNI; National Institutes of Health Grant No. U01 AG024904).

Footnote

Reporting Checklist: The authors have completed the STREGA reporting checklist. Available at https://qims.amegroups.com/article/view/10.21037/qims-22-602/rc

Conflicts of Interest: All authors have completed the ICMJE uniform disclosure form (available at https://qims.amegroups.com/article/view/10.21037/qims-22-602/coif). The authors report that this work was funded by the National Natural Science Foundation of China (Nos. 61971275 and 81830052), the National Key Research and Development Program of China (No. 2020YFC2008700), and the Shanghai Municipal Commission of Science and Technology for Capacity Building for Local Universities (No. 23010502700); data collection and sharing for this project were funded by the Alzheimer's Disease Neuroimaging Initiative (ADNI; National Institutes of Health Grant U01 AG024904). The authors have no other conflicts of interest to declare.

Ethical Statement: The authors are accountable for all aspects of the work in ensuring that questions related to the accuracy or integrity of any part of the work are appropriately investigated and resolved. The study was conducted in accordance with the Declaration of Helsinki (as revised in 2013). This retrospective study was approved by the ethics committee of the Shanghai University of Medicine and Health Sciences, and individual consent for this retrospective analysis was waived.

References

1. Dubois B, Hampel H, Feldman HH, Scheltens P, Aisen

P, Andrieu S, et al. Preclinical Alzheimer's disease: Definition, natural history, and diagnostic criteria. Alzheimers Dement 2016;12:292-323.
2. Alzheimer's Association. 2018 Alzheimer's disease facts and figures. Alzheimer's & Dementia 2018;14:367-429.
3. Hsu S, Gordon BA, Hornbeck R, Norton JB, Levitch D, Louden A, Ziegemeier E, Laforce R Jr, Chhatwal J, Day GS, McDade E, Morris JC, Fagan AM, Benzinger TLS, Goate AM, Cruchaga C, Bateman RJ; Karch CM. Discovery and validation of autosomal dominant Alzheimer's disease mutations. Alzheimers Res Ther 2018;10:67.
4. Zhou T, Thung KH, Zhu X, Shen D. Effective feature learning and fusion of multimodality data using stage-wise deep neural network for dementia diagnosis. Hum Brain Mapp 2019;40:1001-16.
5. Zhu X, Suk HI, Huang H, Shen D. Low-Rank Graph-Regularized Structured Sparse Regression for Identifying Genetic Biomarkers. IEEE Trans Big Data 2017;3:405-14.
6. Yan T, Liang J, Gao J, Wang L, Fujioka H; Zhu X, Wang X. FAM222A encodes a protein which accumulates in plaques in Alzheimer's disease. Nat Commun 2020;11:411.
7. Li JQ, Wang HF, Zhu XC, Sun FR, Tan MS, Tan CC, Jiang T, Tan L, Yu JT; Alzheimer's Disease Neuroimaging Initiative. GWAS-Linked Loci and Neuroimaging Measures in Alzheimer's Disease. Mol Neurobiol 2017;54:146-53.
8. Guo M, Li Y, Zheng W, Huang K, Zhou L, Hu X, Yao Z, Hu B. A novel conversion prediction method of MCI to AD based on longitudinal dynamic morphological features using ADNI structural MRIs. J Neurol 2020;267:2983-97.
9. Lu H; Open Access Series of Imaging Studies. Quantifying Age-Associated Cortical Complexity of Left Dorsolateral Prefrontal Cortex with Multiscale Measurements. J Alzheimers Dis 2020;76:505-16.
10. Wang J, Lyu H, Chen J, Lin S, Zheng H, Li J, Kong F, Gao J, Yu H, Hu Y, Guo Z. Cortical Alterations Are Associated with Depression in Subcortical Vascular Mild Cognitive Impairment Revealed by Surface-Based Morphometry. J Alzheimers Dis 2020;78:673-81.
11. Choi M, Youn H, Kim D, Lee S, Suh S, Seong JK, Jeong HG, Han CE. Comparison of neurodegenerative types using different brain MRI analysis metrics in older adults with normal cognition, mild cognitive impairment, and Alzheimer's dementia. PLoS One 2019;14:e0220739.
12. Yang H, Xu H, Li Q, Jin Y, Jiang W, Wang J, Wu Y, Li W, Yang C, Li X, Xiao S, Shi F, Wang T. Study of brain morphology change in Alzheimer's disease and amnestic mild cognitive impairment compared with normal controls. Gen Psychiatr 2019;32:e100005.
13. Guo XY, Chang Y, Kim Y, Rhee HY, Cho AR, Park S, Ryu CW, San Lee J, Lee KM, Shin W, Park KC, Kim EJ, Jahng GH. Development and evaluation of a T1 standard brain template for Alzheimer disease. Quant Imaging Med Surg 2021;11:2224-44.
14. Lv Y, Zhao W, Yao X, Xu S, Tang Z, Fan Y, Huang G. Analyses of brain cortical changes of Alzheimer's disease. Journal of Mechanics in Medicine and Biology 2021;21:2140025.
15. Shigemizu D, Mitsumori R, Akiyama S, Miyashita A, Morizono T, Higaki S, Asanomi Y, Hara N, Tamiya G, Kinoshita K, Ikeuchi T, Niida S, Ozaki K. Ethnic and trans-ethnic genome-wide association studies identify new loci influencing Japanese Alzheimer's disease risk. Transl Psychiatry 2021;11:151.
16. Jun GR, Chung J, Mez J, Barber R, Beecham GW, Bennett DA, et al. Transethnic genome-wide scan identifies novel Alzheimer's disease loci. Alzheimers Dement 2017;13:727-38.
17. Coon KD, Myers AJ, Craig DW, Webster JA, Pearson JV, Lince DH, et al. A high-density whole-genome association study reveals that APOE is the major susceptibility gene for sporadic late-onset Alzheimer's disease. J Clin Psychiatry 2007;68:613-8.
18. Lambert JC, Ibrahim-Verbaas CA, Harold D, Naj AC, Sims R, Bellenguez C, et al. Meta-analysis of 74,046 individuals identifies 11 new susceptibility loci for Alzheimer's disease. Nat Genet 2013;45:1452-8.
19. Jansen IE, Savage JE, Watanabe K, Bryois J, Williams DM, Steinberg S, et al. Genome-wide meta-analysis identifies new loci and functional pathways influencing Alzheimer's disease risk. Nat Genet 2019;51:404-13.
20. Marioni RE, Harris SE, Zhang Q, McRae AF, Hagenaars SP, Hill WD, Davies G, Ritchie CW, Gale CR, Starr JM, Goate AM, Porteous DJ, Yang J, Evans KL, Deary IJ, Wray NR, Visscher PM. GWAS on family history of Alzheimer's disease. Transl Psychiatry 2018;8:99.
21. Wingo AP, Liu Y, Gerasimov ES, Gockley J, Logsdon BA, Duong DM, Dammer EB, Robins C, Beach TG, Reiman EM, Epstein MP, De Jager PL, Lah JJ, Bennett DA, Seyfried NT, Levey AI, Wingo TS. Integrating human brain proteomes with genome-wide association data implicates new proteins in Alzheimer's disease pathogenesis. Nat Genet 2021;53:143-6.
22. Andrews SJ, Fulton-Howard B, Goate A. Interpretation of risk loci from genome-wide association studies of

Alzheimer's disease. Lancet Neurol 2020;19:326-35.
23. Wachinger C, Nho K, Saykin AJ, Reuter M, Rieckmann A; Alzheimer's Disease Neuroimaging Initiative. A Longitudinal Imaging Genetics Study of Neuroanatomical Asymmetry in Alzheimer's Disease. Biol Psychiatry 2018;84:522-30.
24. Lorenzi M, Altmann A, Gutman B, Wray S, Arber C, Hibar DP, Jahanshad N, Schott JM, Alexander DC, Thompson PM, Ourselin S; Alzheimer's Disease Neuroimaging Initiative. Susceptibility of brain atrophy to TRIB3 in Alzheimer's disease, evidence from functional prioritization in imaging genetics. Proc Natl Acad Sci U S A 2018;115:3162-7.
25. Kim BH, Choi YH, Yang JJ, Kim S, Nho K, Lee JM; Alzheimer's Disease Neuroimaging Initiative. Identification of Novel Genes Associated with Cortical Thickness in Alzheimer's Disease: Systems Biology Approach to Neuroimaging Endophenotype. J Alzheimers Dis 2020;75:531-45.
26. Wu Z, Peng Y, Hong M, Zhang Y. Gray Matter Deterioration Pattern During Alzheimer's Disease Progression: A Regions-of-Interest Based Surface Morphometry Study. Front Aging Neurosci 2021;13:593898.
27. Soheili-Nezhad S, Jahanshad N, Guelfi S, Khosrowabadi R, Saykin AJ, Thompson PM, Beckmann CF, Sprooten E, Zarei M; Alzheimer's Disease Neuroimaging. Imaging genomics discovery of a new risk variant for Alzheimer's disease in the postsynaptic SHARPIN gene. Hum Brain Mapp 2020;41:3737-48.
28. Kim BH, Nho K, Lee JM; Alzheimer's Disease Neuroimaging Initiative. Genome-wide association study identifies susceptibility loci of brain atrophy to NFIA and ST18 in Alzheimer's disease. Neurobiol Aging 2021;102:200.e1-200.e11.
29. Scelsi MA, Khan RR, Lorenzi M, Christopher L, Greicius MD, Schott JM, Ourselin S, Altmann A. Genetic study of multimodal imaging Alzheimer's disease progression score implicates novel loci. Brain 2018;141:2167-80.
30. Meng X, Li J, Zhang Q, Chen F, Bian C, Yao X, Yan J, Xu Z, Risacher SL, Saykin AJ, Liang H, Shen L; Alzheimer's Disease Neuroimaging Initiative. Multivariate genome wide association and network analysis of subcortical imaging phenotypes in Alzheimer's disease. BMC Genomics 2020;21:896.
31. Veitch DP, Weiner MW, Aisen PS, Beckett LA, Cairns NJ, Green RC, Harvey D, Jack CR Jr, Jagust W, Morris JC, Petersen RC, Saykin AJ, Shaw LM, Toga AW, Trojanowski JQ; Alzheimer's Disease Neuroimaging Initiative. Understanding disease progression and improving Alzheimer's disease clinical trials: Recent highlights from the Alzheimer's Disease Neuroimaging Initiative. Alzheimers Dement 2019;15:106-52.
32. Purcell S, Neale B, Todd-Brown K, Thomas L, Ferreira MA, Bender D, Maller J, Sklar P, de Bakker PI, Daly MJ, Sham PC. PLINK: a tool set for whole-genome association and population-based linkage analyses. Am J Hum Genet 2007;81:559-75.
33. Gerretsen P, Chung JK, Shah P, Plitman E, Iwata Y, Caravaggio F, Nakajima S, Pollock BG, Graff-Guerrero A; Alzheimer's Disease Neuroimaging Initiative. Anosognosia Is an Independent Predictor of Conversion From Mild Cognitive Impairment to Alzheimer's Disease and Is Associated With Reduced Brain Metabolism. J Clin Psychiatry 2017;78:e1187-96.
34. Bartos A, Gregus D, Ibrahim I, Tintěra J. Brain volumes and their ratios in Alzheimer´s disease on magnetic resonance imaging segmented using Freesurfer 6.0. Psychiatry Res Neuroimaging 2019;287:70-4.
35. Suresha HS, Parthasarathi SS. Relieff Feature Selection Based Alzheimer Disease Classification using Hybrid Features and Support Vector Machine in Magnetic Resonance Imaging. International Journal of Computer Engineering and Technology 2019;10:124-37.
36. Wu W, Parmar C, Grossmann P, Quackenbush J, Lambin P, Bussink J, Mak R, Aerts HJ. Exploratory Study to Identify Radiomics Classifiers for Lung Cancer Histology. Front Oncol 2016;6:71.
37. Liley J, Wallace C. Accurate error control in high-dimensional association testing using conditional false discovery rates. Biom J 2021;63:1096-130.
38. Yan Y, Zhao A, Qui Y, Li Y, Yan R, Wang Y, Xu W, Deng Y. Genetic Association of FERMT2, HLA-DRB1, CD2AP, and PTK2B Polymorphisms With Alzheimer's Disease Risk in the Southern Chinese Population. Front Aging Neurosci 2020;12:16.
39. Canevelli M, Arisi I, Bacigalupo I, Arighi A, Galimberti D, Vanacore N, D'Onofrio M, Cesari M, Bruno G; Alzheimer's Disease Neuroimaging Initiative. Biomarkers and phenotypic expression in Alzheimer's disease: exploring the contribution of frailty in the Alzheimer's Disease Neuroimaging Initiative. Geroscience 2021;43:1039-51.
40. Zhang Y, Liu S. Analysis of structural brain MRI and multi-parameter classification for Alzheimer's disease. Biomed Tech (Berl) 2018;63:427-37.

41. Youn H, Choi M, Lee S, Kim D, Suh S, Han CE, Jeong HG. Decreased Cortical Thickness and Local Gyrification in Individuals with Subjective Cognitive Impairment. Clin Psychopharmacol Neurosci 2021;19:640-52.
42. Wang RZ, Yang YX, Li HQ, Shen XN, Chen SD, Dong Q, Wang Y, Yu JT; Alzheimer's Disease Neuroimaging Initiative. Genome-Wide Association Study of Brain Alzheimer's Disease-Related Metabolic Decline as Measured by [18F] FDG-PET Imaging. J Alzheimers Dis 2020;77:401-9.
43. Putteeraj M, Fairuz YM, Teoh SL. MicroRNA Dysregulation in Alzheimer's Disease. CNS Neurol Disord Drug Targets 2017;16:1000-9.
44. Shioya M, Obayashi S, Tabunoki H, Arima K, Saito Y, Ishida T, Satoh J. Aberrant microRNA expression in the brains of neurodegenerative diseases: miR-29a decreased in Alzheimer disease brains targets neurone navigator 3. Neuropathol Appl Neurobiol 2010;36:320-30.
45. Yan J, Kim S, Nho K, Chen R, Risacher SL, Moore JH, Saykin AJ, Shen L; Alzheimer's Disease Neuroimaging Initiative. Hippocampal transcriptome-guided genetic analysis of correlated episodic memory phenotypes in Alzheimer's disease. Front Genet 2015;6:117.
46. Xu C, Su BB, Lozano S, Wang K. The neuron navigator 2 gene and Alzheimer's disease. Genetics, Neurology, Behavior, and Diet in Dementia 2020;2:3-24.
47. Choi S, Korstanje R. Proprotein convertases in high-density lipoprotein metabolism. Biomark Res 2013;1:27.
48. Seidah NG, Chrétien M, Mbikay M. The ever-expanding saga of the proprotein convertases and their roles in body homeostasis: emphasis on novel proprotein convertase subtilisin kexin number 9 functions and regulation. Curr Opin Lipidol 2018;29:144-50.
49. Turpeinen H, Seppälä I, Lyytikäinen LP, Raitoharju E, Hutri-Kähönen N, Levula M, Oksala N, Waldenberger M, Klopp N, Illig T, Mononen N, Laaksonen R, Raitakari O, Kähönen M, Lehtimäki T, Pesu M. A genome-wide expression quantitative trait loci analysis of proprotein convertase subtilisin/kexin enzymes identifies a novel regulatory gene variant for FURIN expression and blood pressure. Hum Genet 2015;134:627-36.
50. Chatterjee P, Roy D, Rathi N. Epigenetic Drug Repositioning for Alzheimer's Disease Based on Epigenetic Targets in Human Interactome. J Alzheimers Dis 2018;61:53-65.
51. Cacabelos R, Torrellas C, López-Muñoz F. Epigenomics of Alzheimer's Disease. Journal of Experimental & Clinical Medicine 2014;6:75-82.
52. Romero-Rosales BL, Tamez-Pena JG, Nicolini H, Moreno-Treviño MG, Trevino V. Improving predictive models for Alzheimer's disease using GWAS data by incorporating misclassified samples modeling. PLoS One 2020;15:e0232103.
53. Jo T, Nho K, Saykin AJ. Deep Learning in Alzheimer's Disease: Diagnostic Classification and Prognostic Prediction Using Neuroimaging Data. Front Aging Neurosci 2019;11:220.

Cite this article as: Han L, Jiang H, Yao X, Ren Z, Qu Z, Yu T, Luo S, Wu T. Revealing the correlations between brain cortical characteristics and susceptibility genes for Alzheimer disease: a cross-sectional study. Quant Imaging Med Surg 2023;13(4):2451-2465. doi: 10.21037/qims-22-602

